

Morphology, Thermal and Impedance Characteristics of Iodine Doped Metal Iodide-Epoxidized Natural Rubber (MI-ENR) Polymer Electrolytes

W.L.Tan^{*}, M. Abu Bakar

School of Chemical Sciences, Universiti Sains Malaysia, 11800 Penang, Malaysia.

*E-mail: weileng728@gmail.com; weileng_tan@usm.my

Received: 7 June 2016 / Accepted: 29 July 2016 / Published: 6 September 2016

A series of metal iodide-epoxidized natural rubber (MI-ENR) (where M= Li, Na, K or Ag) and their iodine (I₂) doped derivative (I₂/MI-ENR) polymer electrolytes (PEs) were successfully prepared via solvent casting method. The PEs were characterized using UV-vis, FTIR and SEM/X-mapping techniques. Their thermal properties were studied using DSC and TG analysis while the ionic conductivity characteristic was evaluated using the impedance spectroscopy. The glass transition temperature (T_g) and impedance characteristics of the MI-ENR PEs is dependent on the solubility of MI salt in the ENR, the interaction of MI with ENR and the outcome morphology of the PE. The alkali metal iodides, MI (M= Li, Na or K) do not affect the thermal stability of ENR in the respective PEs. However, the AgI destabilized the ENR in the AgI-ENR PE. Doping the MI-ENR PEs with I₂, caused increment in T_g, enhancement in thermal stability and changed the conduction mechanism.

Keywords: ENR, iodine, polymer electrolyte, metal iodide, thermal, impedance

1. INTRODUCTION

Polymer electrolyte (PE) is an ionic conductor. It is one of the key constituents in electrochromic devices, capacitors, batteries, sensors, fuel cells and dye-sensitized solar cells (DSSCs) [1]. It is prepared by adding metal salt into a polymer host. The superior performance of the PE over conventional liquid electrolyte lies in the fact that it is lighter, safer, more flexible and stable in terms of thermal and mechanical aspects.

The Li⁺ ion is light and possesses high energy and power density [2]. Therefore lithium salt (LiX) is the most common source of Li⁺ ion charge carrier hence is widely applied in PEs. Examples include; Li⁺-poly(ethylene oxide) (PEO) [3], Li⁺-epoxidized natural rubber (ENR) [4], Li⁺-poly(vinyl

chloride) (PVC) [5], Li⁺-cellulose acetate [6] and many more. Other metal ion (Mⁿ⁺) charge carriers are also known. The sodium ion (Na⁺) [7,8], zinc ion (Zn²⁺) [9], silver ion (Ag⁺) [10,11], potassium ion (K⁺) [12,13] and magnesium ion (Mg²⁺) [14] are some examples. The conductivity of these ions has been ascertained to be at par with Li⁺ ions.

ENR is a chemically modified natural rubber (NR) [15]. ENR possesses some interesting characteristics such as low glass transition temperature (T_g), random distribution of polar epoxide group, high tensile strength, good elasticity and adhesion [15]. This makes ENR an ideal candidate for PE applications. ENR-based PE has been extensively reported. To date, research work on ENR-based PEs has been limited mostly to Li salts. Earliest study on Li⁺-ENR PEs was reported by Idris et al. [4,16]. In one of their studies, they prepared a series of PE constituting plasticized and unplasticized ENR containing lithium triflate (LiCF₃SO₃) and reported the thermal properties and ionic conductivities. Later, Klinklai and co-workers [17,18] reported the effect of protein and epoxidation level of ENR on the thermal and electrical properties of ENR/bis(trifluoromethane sulfonyl)imide (LiTFSI) PEs. Mohamed et al. [19] constructed lithium-air cells comprising of ENR-based PE. ENR has also been blended with others polymer such as PEO [16,20,21], poly(methyl methacrylate) (PMMA) [22], and PVC [23,24] or grafted with carboxyl ionic liquid [25] for use as base matrix in PE. Our group has reported the effect of different anions of lithium salt on the property of LiX-ENR (where X = CF₃SO₃⁻, COOCF₃⁻, I⁻, BF₄⁻ and ClO₄⁻) PEs [26, 27]. It was found that the thermal, morphological and ionic conductivity of the PEs is dependent on the types of anion of the LiX salt. Recently, we have also demonstrated that the incorporation of Fe₃O₄ nanoparticles can further alter their properties [28,29].

Iodine (I₂) is sometimes added to the metal iodide (MI)-polymer PE systems in order to further tailor the conducting performance of the PE [13,14]. The I₂/MI-polymer PE is deemed suitable for DSSC application. The I₂ combines with I⁻ to form I₃⁻ and this produces an I⁻/I₃⁻ redox couple which facilitates electron transfer to the dye in the DSSC. Numerous I₂/MI-polymer systems including I₂/NaI-poly(acrylonitrile-*co*-styrene) [8], I₂/KI-PEO-succinonitrile [13], I₂/MgI₂-poly-ethylene glycol [14], I₂/LiI-agarose [30] and the likes have been reported. Thus far, there is scarcely any report on I₂/MI-ENR PEs. Henceforth, we report the synthesis, thermal and impedance properties of a series of MI-ENR (where M = Li, Na, K and Ag) and their respective iodine doped I₂/MI-ENR PEs.

2. EXPERIMENTAL

2.1. Materials

All the chemicals were obtained commercially and used as received without further purification unless otherwise stated. Potassium iodide (KI) 99%, sodium iodide (NaI) 99.5% and silver iodide (AgI) 99% were purchased from Sigma-Aldrich, USA. Lithium iodide (LiI) 99% was obtained from Acros Organic, USA. Iodine (I₂), resublimed and ethanol were from R&M Chemicals, UK. Tetrahydrofuran (THF) was from Merck, Germany. Epoxidized natural rubber with 50% epoxidation

was obtained from Guthrie Polymer (Malaysia) Sdn. Bhd. and was purified according to the literature [31] before used.

2.2. Methods

2.2.1. Preparation of MI-ENR PEs

Solvent casting method was adopted to prepare the respective samples. Typically, the metal iodide, MI (where M = Li, Na, K and Ag) of various amounts (5 to 25 wt% w.r.t. ENR) was weighed and dissolved in 4 mL THF (or ethanol in the case of AgI). Then 0.25 g of ENR in 5 mL THF solution was added while vigorously stirring. The solution was topped up to 10 mL with THF. The solution mixture was stirred for 2 h. Then the solution was cast into a Teflon mould and left to dry in air to form a film. The sample was further dried in a vacuum oven at 50°C overnight.

2.2.2. Preparation of I₂/MI-ENR PEs

The preparation of the I₂/MI-ENR PEs was similar to the preparation of MI-ENR samples as described above. However, for the I₂/MI-ENR samples, the base PE of MI-ENR each containing 10 wt% (wrt ENR) of MI salt was used. The typical preparation of I₂/MI-ENR PE is as follows; 25.0 mg of the MI salt was weighed and dissolved in 4 mL THF (or ethanol in the case of AgI). Then 0.25 g of ENR in 5 mL THF solution was added while vigorously stirring. The I₂ in THF solution of various weight ratios (w.r.t. MI salt) was added into the above solution. The solution was topped up with THF to a total of 10 mL. Stirring was continued for 2 h. Lastly, the solution was cast into a Teflon mould and left to dry in air to form a film. The obtained film was further dried in a vacuum oven at 50°C overnight.

2.3. Characterization

UV-vis spectroscopy was utilized to study the iodide species that were present in the samples. A Hitachi U-2000 spectrophotometer was employed to record the UV-vis absorption spectra of the sample solutions. The spectra were scanned from 200 to 800 nm and THF was used as the reference. The FTIR spectra were recorded using a Perkin-Elmer 2000 infrared spectrometer. The sample solution was drop cast onto a ZnSe window to form a thin film. The spectra were collected in the region of 4000 to 650 cm⁻¹. The SEM and X-mapping micrographs were obtained using a Leo Supra 50VP Field Emission Scanning Electron Microscope (FE-SEM). The samples were coated with a layer of gold prior to analysis. The thermal properties of PEs were studied using a Perkin Elmer Pyris differential scanning calorimeter (DSC) and a Perkin Elmer TGA-7 thermogravimetry (TG). In DSC analyses, ~10 mg of the sample was weighed and sealed in an aluminum pan. Sample was first heated from -50 to 100°C at a heating rate of 20 °C min⁻¹ and the final temperature was held for 3 mins. It was then quenched to -50°C at a rate of 100 °C min⁻¹. The sample was subjected to a second heating scan

where it was again heated to 100°C at a similar heating rate of 20 °C min⁻¹. The glass transition temperature (T_g) was obtained from the inflection point in the thermogram of the second heating scan using a Pyris 1 DSC software. For TG analysis, ~10 mg of the sample was weighed and heated from room temperature to 600°C at 20 °C min⁻¹ under nitrogen environment. The onset temperature (T_{onset}) of the thermal decomposition, defined as the intersection point between the linear extrapolation of the baseline and their fitted maximum slope of the TG curve, was acquired from the computer program STARe (version 9.20) software. The ionic conductivity of the sample was studied using an electrochemical impedance spectroscopy (EIS) GAMRY Reference 600 potentiostat/galvanostat/ZRA. The sample was subjected to the frequency range of 1 Hz to 1 MHz at 10 mV amplitude. The Nyquist plot was fitted using a ZSimDemo 3.22d software to obtain the equivalent circuit.

3. RESULTS AND DISCUSSION

3.1. Characterization

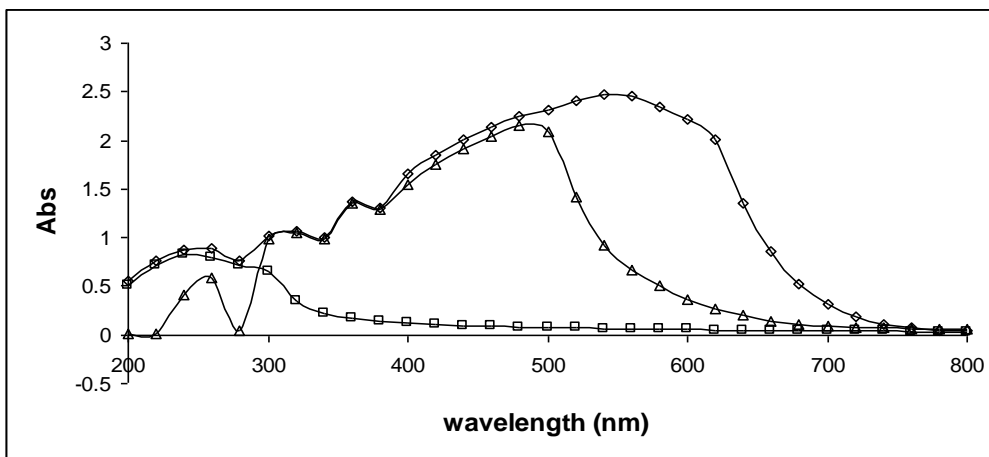
3.1.1. UV-vis Spectroscopy

The KI and AgI hardly dissolved in the ENR/THF solution. Nevertheless, the solubility of KI can be enhanced by adding few drops of ethanol. The AgI, on the other hand, was insoluble even after a large amount of ethanol has been added. The MI-ENR (where M = Li, Na, K or Ag) THF solutions were yellow in color. Addition of I₂ into the MI-ENR solutions intensified the color of the resultant solution to brown depending on the amount of I₂ added.

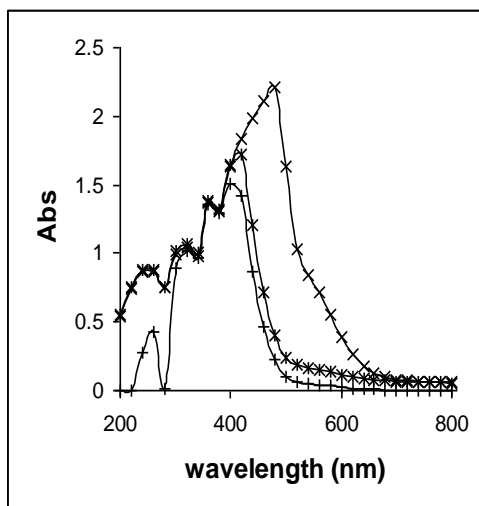
In water, the λ_{max} for iodine (I₂) is at ~220 nm, the monoiodide (I⁻) at ~190-200 nm and ~230 nm, triiodide (I₃⁻) at ~290-310 nm and ~350 nm, pentaoidide (I₅⁻) at ~270 nm and ~360-375 nm as well as polyiodide (I_n⁻ where n >5) at ~590 nm and ~620 nm [32-34]. In THF however, the λ_{max} for I⁻ is at 254 nm [35]. The difference in the λ_{max} w.r.t. those in water can be attributed to the increase in refractive index (n) of the medium, that is, the transition from water ($n_{water}=1.33$) to THF ($n_{THF}=1.4$). Similar phenomena have been observed in other works [33,34,36].

The UV-vis absorption spectra of purified ENR, I₂ and I₂/ENR THF solutions are shown in Figure 1(a). The purified ENR exhibits a broad peak carrying a shoulder with λ_{max} at 246 nm and 292 nm respectively. The I₂ showed four peaks with λ_{max} at 250 nm, 312 nm, 371 nm and 549 nm and are attributed to the existence of I⁻, I₃⁻, I₅⁻ and some polyiodide species respectively. The UV spectrum for I₂/ENR also exhibits 4 peaks. These are 252, 313, 371 and 487 nm. The first 3 peaks are located at positions that are similar to iodine which corresponds to I⁻, I₃⁻ and I₅⁻. The peak at 487 nm on the other hand maybe due to the formation of ENR-iodide complex in the sample. Shin and co-workers [33,34] have observed similar UV-vis peak profile in the I₂/KI-PVA at ~470-480 nm and ~600-650 nm respectively and attribute the respective peak to the PVA-I₃⁻ and PVA-I₅⁻ complexes. In the present work, analogues corresponding peaks may be appropriated to the presence of ENR-iodide complexes i.e. ENR-I₃⁻ or ENR-I₅⁻ respectively.

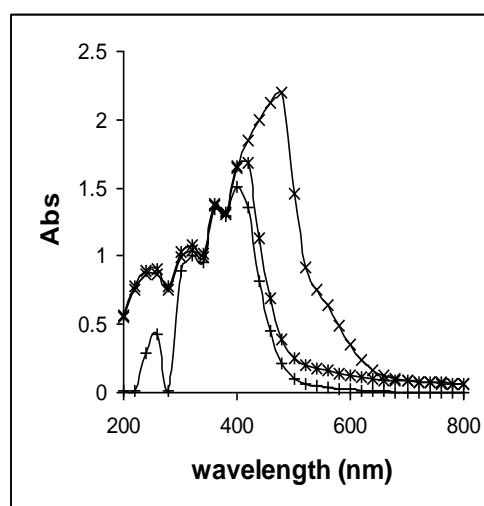
With the exception of AgI-ENR, other MI-ENR show 4 peaks at λ_{max} 250 nm, 312 nm, 371 nm and ~413 nm. The first 3 peaks are similar to those of I₂/ENR and are assignable to I⁻, I₃⁻ and I₅⁻ species, whereas the peak at 412-415 nm may be due to the existence of polyiodide species.



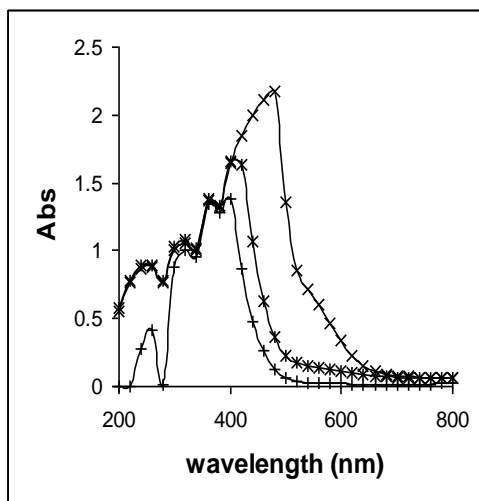
a)



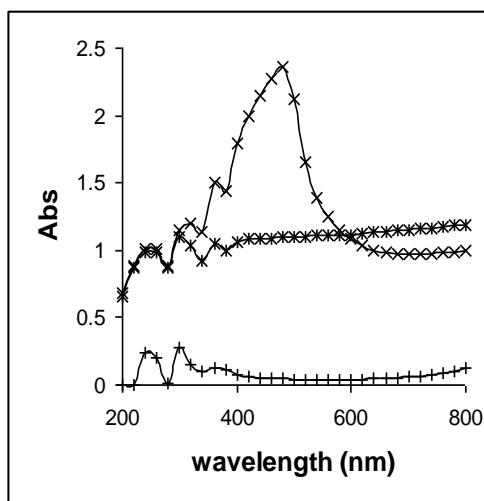
b)



c)



d)



e)

Figure 1. UV-vis spectra for the THF solutions of (a) ENR (□), I₂ (◇) and I₂/ENR (Δ) and the various MI (+), MI-ENR (*) and I₂/MI-ENR (x) with M = (b) Li, (c) Na, (d) K and (e) Ag.

The AgI-ENR however, exhibits 3 peaks with λ_{max} of 249 nm, 307 nm and 362 nm. The former peak is assigned to Γ while the later two are most probably due to the excitonic/interband transition of

AgI particles [37]. The UV-vis spectra for all the I₂/MI-ENR also exhibit 3 narrow peaks at wavelength < 400 nm with the λ_{max} at 250 nm, 313 nm and 372 nm indicating the existence of I⁻, I₃⁻ and I₅⁻ in the solution. There was also a broad peak ranging from 400-700 nm with a maximum at ~477-484 nm and a shoulder at ~540 nm that are assignable to the presence of ENR-I₃⁻ and ENR-I₅⁻ respectively.

3.1.2. FTIR Spectroscopy

The FTIR spectra of the pristine ENR, various MI-ENR and I₂/MI-ENR PEs are shown in Figure 2. The peaks and their corresponding assignments are tabulated in Table 1. As shown in Figure 2(a), the spectrum of pristine ENR demonstrates similar features to those reported in previous works [26]. These include C-H symmetric and asymmetric stretching at 2700-3000 cm⁻¹, the C-H deformation at 1453 and 1377 cm⁻¹, the C=C stretching and =C-H bending at 1660 and 837 cm⁻¹ respectively as well as epoxide ring ($\overset{\text{O}}{\underset{\text{C}}{\text{C}}}$) asymmetrical stretching at 877 cm⁻¹. The spectra of MI-ENR PEs (Figure 2(b-e)) exhibit similar peaks as the spectrum of pristine ENR. These peaks are the C-H stretching and deformation as well as the characteristic C=C and epoxide. However, an additional two intense peaks which attributed to the H₂O in the samples are observed at ~3400 and ~1640 cm⁻¹. The intensity of these peaks decreases in the order of AgI < KI < NaI < LiI and is in accordance to the hygroscopic tendency of the respective salt. The polar ($\overset{\text{O}}{\underset{\text{C}}{\text{C}}}$) of ENR is the most possible interaction sites for cations [17,18]. The ($\overset{\text{O}}{\underset{\text{C}}{\text{C}}}$) asymmetrical ring stretching is located at 876-877 cm⁻¹. For AgI-, KI- and NaI-ENR PEs, the position of this peak does not change w.r.t. ENR. However, in the LiI-ENR PE, the $\overset{\text{O}}{\underset{\text{C}}{\text{C}}}$ peak was slightly shifted to 874 cm⁻¹. The peak was further shifted to a lower wavenumber as the loading of LiI is increased. For example, the $\overset{\text{O}}{\underset{\text{C}}{\text{C}}}$ peak of 25 wt% LiI-ENR is at 872 cm⁻¹. The shift in the $\overset{\text{O}}{\underset{\text{C}}{\text{C}}}$ peak reveals the extent of complexation between the iodide salts and ENR within the PE. Obviously, apart from the LiI-ENR, there is barely any complexation between the AgI, KI or NaI and the ENR. Apart from that, the position of the C=C stretching peak for MI-ENR PEs with M = Li and Na merge with the O-H bending of the adsorbed moisture, thus only a broad peak centred at 1634 and 1625 cm⁻¹ is observed respectively.

Table 1. FTIR peak positions and assignments for pristine ENR and various PEs.

sample	Assignments and peak position (cm ⁻¹)								
	ν_{as} (C-H)	ν_{s} (C-H)	C-H bending	ν_{s} (C-O-C)	ν_{as} (C-O-C)	ν_{as} (C=C)	=C-H bending	O-H	C=O
Neat ENR	2964, 2926	2862	1379, 1454	1256	877	1665	837	3469	-
M ⁺ T-ENR, M =									
(a) Li	2965, 2926	2861	1380, 1458	1255	874	1634	838	3434	-
(b) Na	2964, 2926	2862	1379, 1454	1256	876	1625	838	3468	-
(c) K	2964, 2926	2862	1379, 1453	1256	877	1662	837	3469	-
(d) Ag	2964, 2926	2861	1379, 1453	1257	877	1665	838	3481	-
I ₂ /M ⁺ T-ENR, M=									
(a) Li	2964, 2927	2861	1379, 1455	1259	873	1644	838	3446	1709
(b) Na	2964, 2927	2861	1379, 1453	1259	875	1627	838	3461	1725
(c) K	2963, 2925	2860	1378, 1452	1252	873	1663	839	3468	1712
(d) Ag	2964, 2928	2861	1378, 1455	1250	873	1664	839	3460	1711

As shown in the red overlay in Figure 2, the most significant difference between the PEs of MI-ENR and I₂/MI-ENR is the appearance of new peak at ~1710 cm⁻¹ which is assignable to the stretching of C=O [38]. Possible origin of this peak is explained below. Besides, the symmetrical and asymmetrical stretching of C-O-C epoxide ring were also shifted as compared to pristine ENR as well as their respective undoped counterparts. The shift is ~4-6 cm⁻¹. In the case of C=C and =C-H stretching, the position for I₂/MI-ENR is similar to their undoped PEs. Previous works have shown that the I₂ molecules are able to interact with moieties like C=C, nitrogen or oxygen atoms to form complexes [39-42]. In some cases, the I₂ can even induce oxidation by accepting an electron be converted to I⁻ [43,44]. In this present work, it is envisaged that the I₂ favourably interacts with the oxygen atom of the epoxide ring rather than the C=C bond in the ENR chains. By doing so, it induced some oxidation of the ENR as evident by the presence of the C=O stretching peak described above.

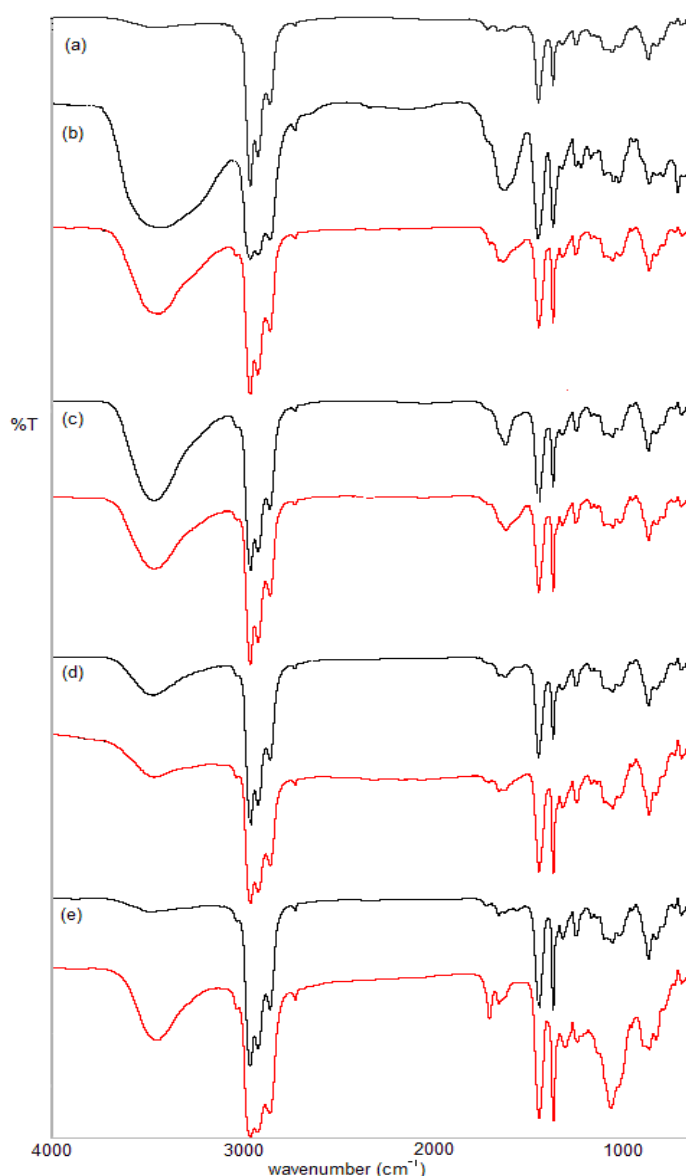


Figure 2. Typical FTIR spectra for (a) ENR and the various 10 wt% MI-ENR and I₂/MI-ENR (red overlay) PEs where M = (b) Li, (c) Na, (d) K and (e) Ag.

3.2. Surface Morphology

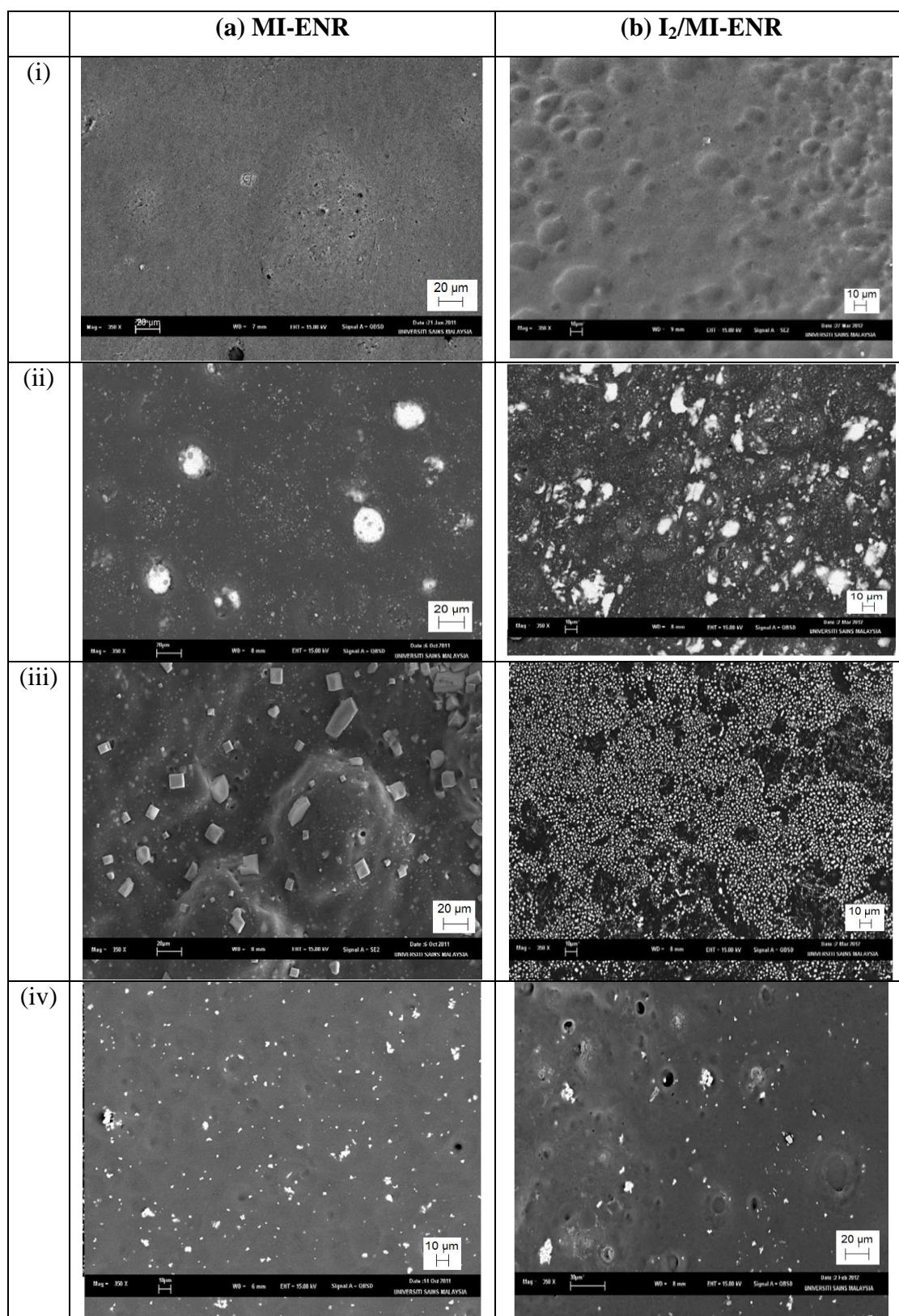


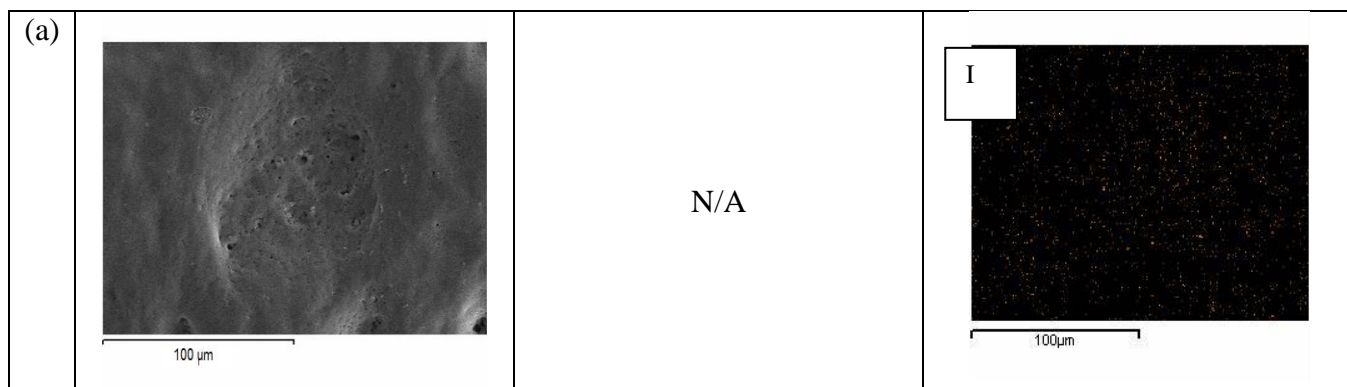
Figure 3. SEM micrographs with magnification of 350 x for (a) 10 wt% MI-ENR and (b) I₂/MI-ENR PEs where M = (i) Li, (ii) Na, (iii) K and (iv) Ag.

The SEM micrographs of MI-ENR and I₂/MI-ENR PEs are shown in Figure 3. In the LiI-ENR, the salt seems to be well solvated in the ENR matrix where no phase separation was observed in the SEM micrograph (Figure 3(a)(i)). Likewise, other LiI-polymer electrolyte systems with similar LiI salt content also gave smooth surface morphology [45,46]. However, salt particles with some aggregation are visible in the SEM micrographs of NaI- (Figure 3(b)(i)), KI- (Figure 3(c)(i)) and AgI-ENR PE (Figure 3(d)(i)). Thus, these iodide salts are less solvated in the ENR matrix as compared to LiI. The NaI and AgI particles showed irregular shape while most of the KI particles are mostly cube shape. A similar surface morphology in which phase separation occurred between NaI-, KI- and AgI-polymer systems were also previously reported [12,47,48].

The I₂/LiI-ENR and I₂/AgI-ENR PEs exhibit similar surface morphology compared to their undoped counterparts while the I₂/NaI-ENR and I₂/KI-ENR PEs show distinct differences. The I₂/LiI-ENR (Figure 3(a)(ii)) exhibited a smooth surface while the surface of I₂/AgI-ENR (Figure 3(d)(ii)) comprised of irregular AgI particles distributed on the surface. The surface of the I₂/NaI-ENR (Figure 3(b)(ii)) consists of irregular salt granulates that spread all over the ENR matrix. The granulate density is higher than that of the NaI-ENR. The I₂/KI-ENR (Figure 3(c)(ii)) displays even more interesting morphology where the cube shaped KI particles are very small and well packed throughout the surface.

The distribution of iodide salts in ENR for each PE sample was further studied by element mapping and the corresponding micrographs are illustrated in Figure 4. As shown in Figure 4(a), the element I is distributed throughout the matrix. Thus, LiI is evenly distributed in the ENR. The component elements of the respective NaI, KI and AgI in the PEs are shown in Figure 4(b-d). In this case of NaI- and KI-ENR PEs, there are mixtures of big and small salt particles, as displayed by respective bright and light contrast, distributed all over the ENR matrix. Nevertheless, the AgI particles in the PE are mostly aggregated in large isolated clusters.

The element mapping micrographs for the corresponding I₂ doped samples are shown in Figure 5. For the I₂/LiI-ENR (Figure 5(a)), the micrograph displayed color contrast that was almost identical throughout. Therefore, the element I was homogeneously distributed over the surface. For the I₂/NaI-ENR (Figure 5(b)) and I₂/KI-ENR (Figure 5(c)), the respective NaI and KI particles are distributed throughout the surface. However, in the I₂/AgI-ENR (Figure 5(d)), the AgI particles seem more agglomerated.



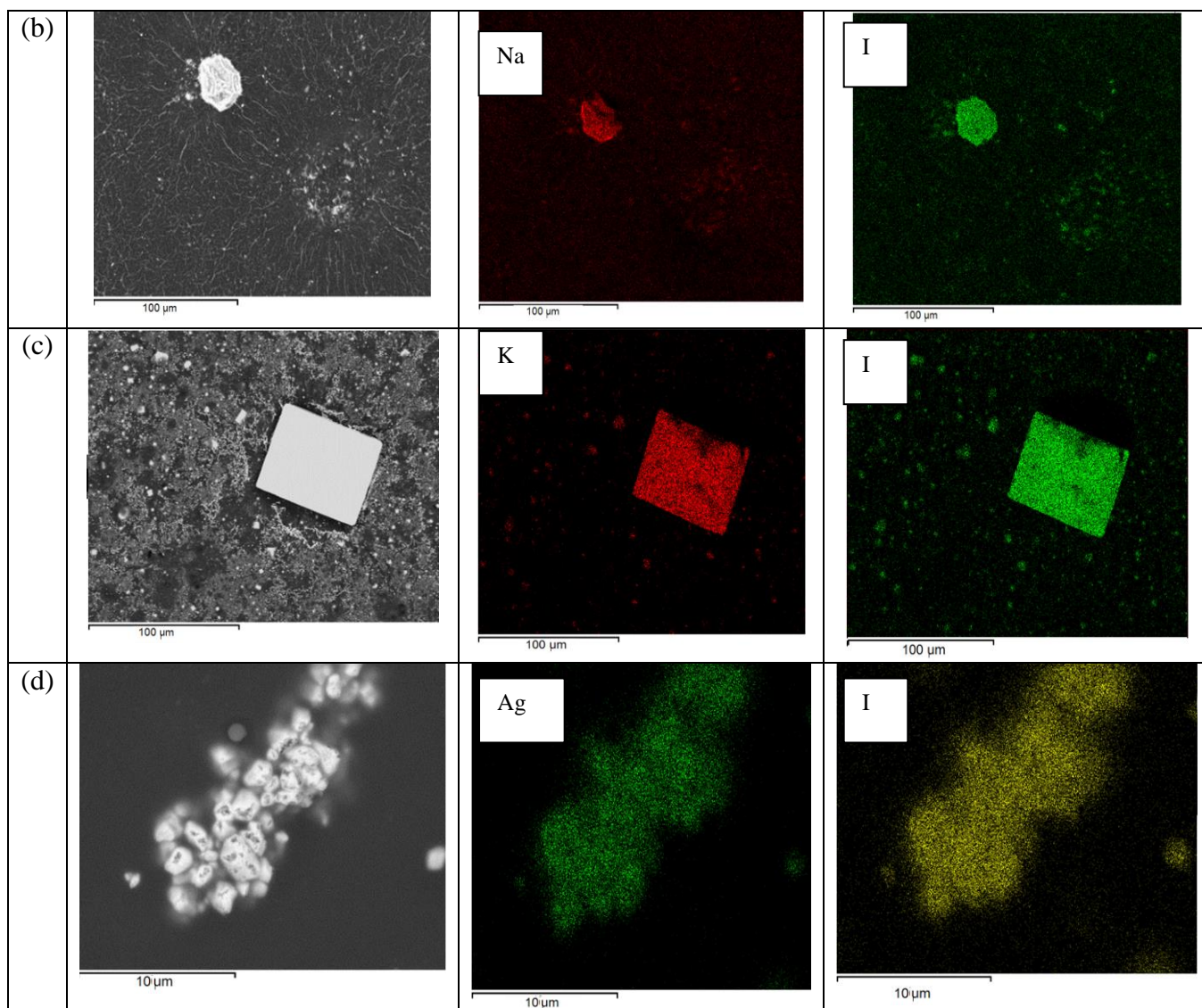
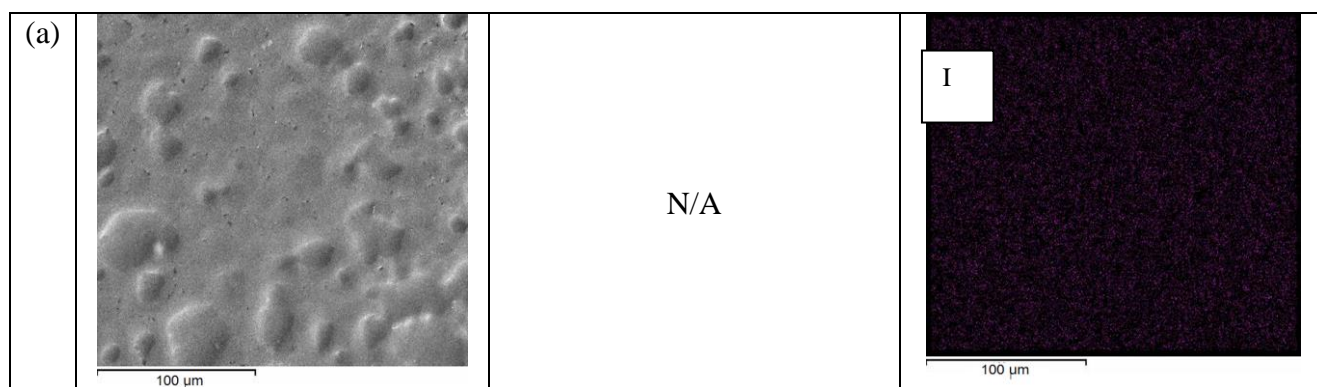


Figure 4. Element mapping micrographs for 10 wt% MI-ENR PEs where M = (a) Li, (b) Na, (c) K and (d) Ag.



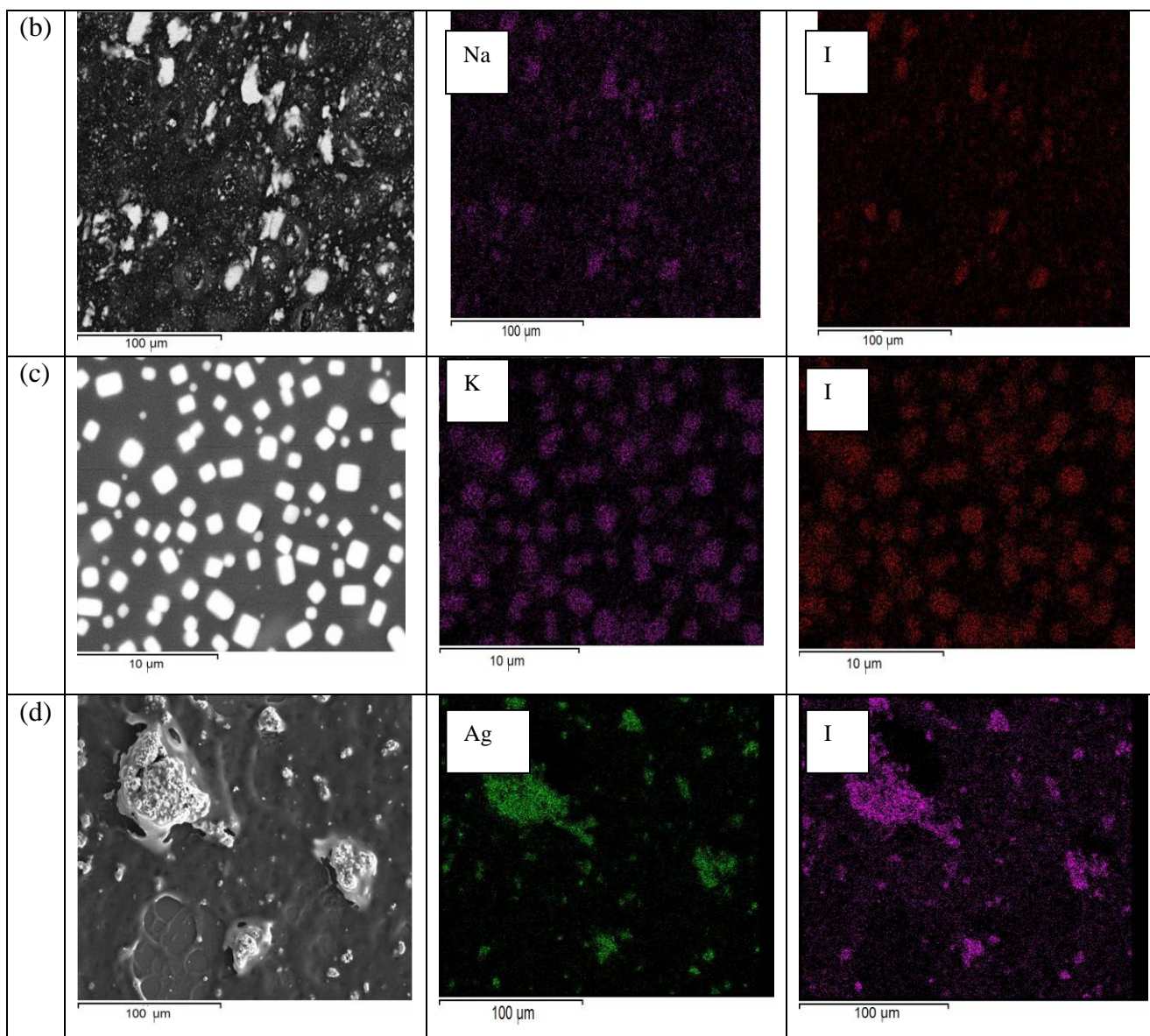


Figure 5. Element mapping micrographs for I_2 doped 10 wt% MI-ENR PEs where M = (a) Li, (b) Na, (c) K and (d) Ag.

Overall, the surface morphology of the samples correlates to the extent of interaction between the ENR and MI salts. As revealed by the FTIR results, ENR may exerts a moderate interaction to LiI. This creates LiI-ENR complexation that help to solvate the LiI salt in the ENR matrix. Hence, a smooth surface is obtained. Similar findings were found elsewhere [45,46]. In contrast, there is barely any interaction between the ENR and NaI, KI or AgI. These MI salts are less solvated in the ENR matrix and caused phase separation or aggregation to occur. Similar observation was found in the PE system comprised of NaI-hydroxypropyl methylcellulose (HPMC) [47] as well as AgI-penton [48].

3.3. Thermal Behaviours

3.3.1. DSC

Except for the LiI-ENR, the thin film of MI-ENR or I₂/MI-ENR PE retained the flexibility and stickiness of the ENR. This can be explained by the extent of interactions between the salt and ENR [26]. The T_g of the PEs are tabulated in Table 2. Regardless of the salt loading in ENR, the T_g for NaI-, KI- and AgI-ENR are within the range of -18 to -17°C and are close to the pristine ENR (T_g = -19 °C). In contrary, the LiI-ENR showed a much higher T_g as compared to pristine ENR or the other MI-ENR PEs. Furthermore, the T_g of LiI-ENR also increases with the increase in wt% of LiI. For instance, the T_g for ENR with 5, 10 and 20 wt% of LiI is -15.0, -7.7 and -5.0 °C respectively. The increment of T_g upon adding the LiI into ENR is due to the pseudo-crosslinking between the Li⁺ and ENR chains that consequently restrict the mobility of ENR chains [4,16]. Thus higher T_g values are observed. For other iodide salts (M = Na, K or Ag), the slight T_g increment in their respective PEs from pristine ENR, infers weaker interaction occurring between the salt and ENR.

The I₂/MI-ENR PE films are more rigid than their undoped counterparts. The corresponding T_g results are shown in Table 2. In general, the T_g of PEs doped with I₂ is higher than undoped samples and increases with the increase of I₂. For instance, the T_g of MI-ENR PE doped with I₂ at the ratio of 1.0 was -10.2, -10.3, -10.2 and 6.5 °C for M=Li, Na, K and Ag respectively. Doping of I₂ in the PE systems promoted the formation of ENR-iodide complex ions as suggested by the UV-vis and FTIR results discussed above. Hence, the complexation between the ENR and iodide ions confines the movement of the ENR chains and thus causes an increment in T_g value.

Table 2. Glass transition temperature (T_g) for various PEs.

wt % of MI (w.r.t. ENR)	Ratio of I ₂ :MI	Li	Na	K	Ag
0*	-	-19.0	-19.0	-19.0	-19.0
5	-	-15.0	-17.4	-18.0	-18.0
10	0.0	-13.3	-17.4	-18.2	-18.4
10	0.1	-14.9	-16.5	-17.4	-16.6
10	0.5	-16.3	-16.6	-16.6	-10.3
10	1.0	-10.2	-10.3	-10.2	6.5
15	-	-7.7	-17.1	-18.3	-17.7
20	-	-5.0	-16.8	-18.3	-18.4
25	-	-7.7	-17.2	-18.2	-18.3

Note: * pristine ENR.

3.3.2. TG Analysis

The TG and DTG curves for pristine ENR and the representative 10 wt% MI-ENR PEs are depicted in Figure 6(a) and 6(b). In the TG curve of pristine ENR, only one weight loss that starts at ~375°C is observed. Its maximum weight loss is located at 397°C as shown in the DTG curve. LiI- and NaI-ENR shows a different TG profile from pristine ENR. They demonstrated two major weight loss

stages in TG thus two DTG peaks were observed. The first weight loss of LiI- or NaI-ENR ranges from 180-220°C and 110-170°C with 9% and 6% weight loss respectively. This stage of weight loss can be attributed to the decomposition of the respective thermally less stable hydrated iodide salt ($MI \cdot xH_2O$) [26] in the PE. The second weight loss is due to the decomposition of ENR in the PE. The decomposition started at $\sim 375^\circ\text{C}$ and $\sim 372^\circ\text{C}$ for ENR incorporated with LiI and NaI respectively. On the other hand, KI- and AgI-ENR only exerted one weight loss stage with one DTG peak which is similar to pristine ENR. The decomposition was between ~ 380 - 440°C and ~ 360 - 455°C respectively.

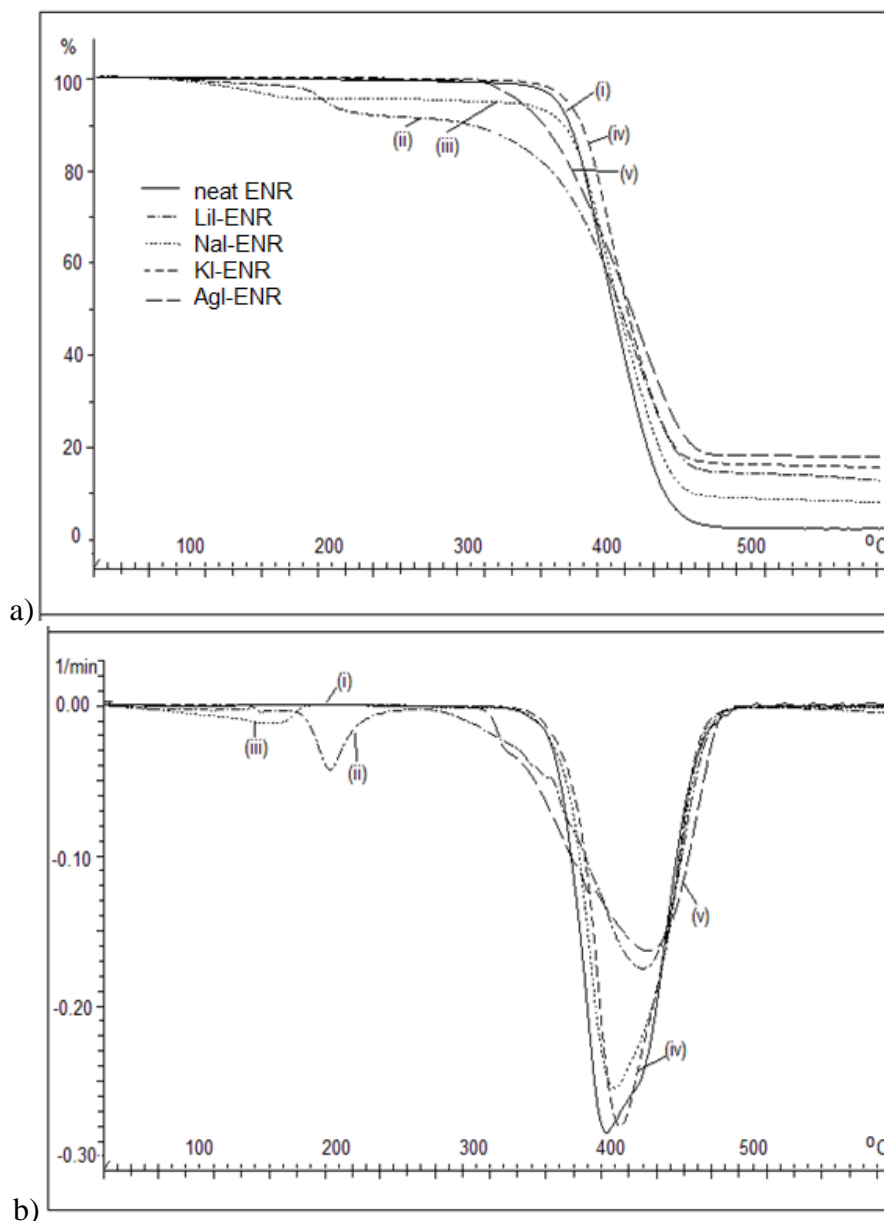


Figure 6. (a) TG and (b) DTG curves for (i) ENR and the various 10 wt% MI-ENR where M = (ii) Li, (iii) Na, (iv) K and (v) Ag (heating rate: $20^\circ\text{C min}^{-1}$).

Apart from the AgI-ENR, the other MI-ENR PEs showed comparable onset temperature (T_{onset}) for the decomposition of ENR to pristine ENR. Therefore, these MI salts do not significantly affect the

stability of ENR in the PE. The T_{onset} for the AgI-ENR was $\sim 15^{\circ}\text{C}$ lower than pristine ENR. This suggests that the presence of AgI in the PE destabilized the ENR and caused its decomposition to occur earlier. In a previous study [49], it was shown that silver sulfide (Ag_2S) particles catalyzed the thermal degradation of poly(3-hydroxybutyrate) (PHB) via an effective heat transfer between the particle surface and polymers. It is envisaged that the AgI particles in the AgI-ENR PE also exert a similar role as Ag_2S particles, hence promoting the degradation of ENR.

To further understand the effect of concentration of iodide salt to the decomposition of ENR in the PE, the graph of T_{onset} versus wt% of iodide salt in the PE was constructed. As shown in Figure 7, the T_{onset} for NaI-, KI- and AgI-ENR PEs remains constant for PE containing 5 to 25 wt% of salt. However, the T_{onset} for LiI-ENR is dependent on the LiI loading. The T_{onset} for PE with 5 wt% of LiI is 369°C . This increases to 375°C to 385°C and to 396°C for LiI loadings of 10, 15 and 20 wt% respectively. The T_{onset} slightly decreases to 392°C upon further increment of LiI loading to 25 wt%. The trend may be explained by the solubility and interaction between the iodide salt and ENR. The NaI, KI and AgI hardly dissolved in the ENR matrix. Thus barely any interaction between the salt and ENR existed although the wt% of salt was increased. Consequently, the T_{onset} stays constant throughout a range of salt loading. For LiI-ENR PEs, the amount of Li^+ increase as the wt% of LiI is increased from 5 to 20. Ultimately, more pseudo-crosslinking are formed between the Li^+ and ENR [26]. This interaction gives higher thermal stability to the PE which is reflected by the higher T_{onset} . Nevertheless, for the PE with 25 wt% of LiI, the formation of salt aggregation reduces the quantity of Li^+ available that eventually reduces the crosslinking and T_{onset} . The trend of T_{onset} with respect to the wt% of MI is similar to T_g 's trend obtained by DSC analysis.

Figure 8 shows the TG and DTG curves of the various I_2/MI -ENR PEs at a heating rate of $20^{\circ}\text{C min}^{-1}$. Generally, the doped PEs displayed 2 distinct weight losses at $160\text{-}230^{\circ}\text{C}$ and $380\text{-}480^{\circ}\text{C}$ as shown in the TG curves (Figure 8(a)). The first weight loss is due to the liberation of I_2 [50] while the second weight loss is attributed to the decomposition of ENR [26,27] in the samples. The DTG peaks related to these weight losses are shown in Figure 8(b). It should be noted that the DTG peak at $160\text{-}230^{\circ}\text{C}$ for LiI and NaI is broad but is sharp for KI and AgI. As mentioned earlier, hydrated salts of LiI and NaI in the PEs decomposes at around $110\text{-}220^{\circ}\text{C}$. Hence, it is believed that the broadness of the peak, in the case of LiI and NaI, is due to the superposition of the decomposition of hydrated iodide salt and the vaporization of I_2 . Apart from that, some minor weight loss ($< 3\%$) also occurs at $< 150^{\circ}\text{C}$ for I_2 doped LiI- and NaI-ENR PEs. This is represented by a very small but broad DTG peak. This stage of weight loss is related to the evaporation of trapped moisture. The ENR started to decompose at $\sim 406^{\circ}\text{C}$, $\sim 413^{\circ}\text{C}$, $\sim 394^{\circ}\text{C}$ and $\sim 402^{\circ}\text{C}$ for I_2 doped MI-ENR PEs where $\text{M} = \text{Li}, \text{Na}, \text{K}$ and Ag respectively. The T_{onset} shifted to ca. $\sim 20^{\circ}\text{C}$ higher than ENR and the respective undoped PEs. Apparently, doping I_2 into the MI-ENR PEs caused higher thermal stability as compared to their undoped counterparts. This superior thermal property may be due to the formation of ENR-iodide complexes in the doped PEs.

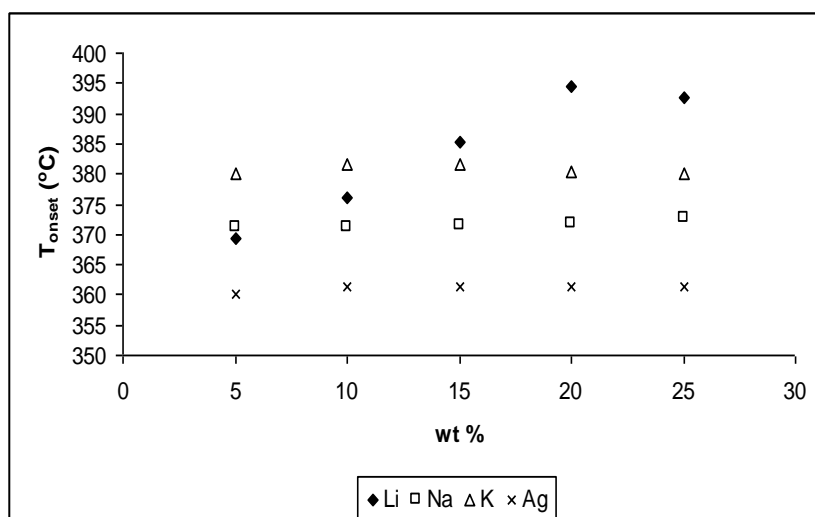


Figure 7. Variation of T_{onset} with wt % of salt in MI-ENR.

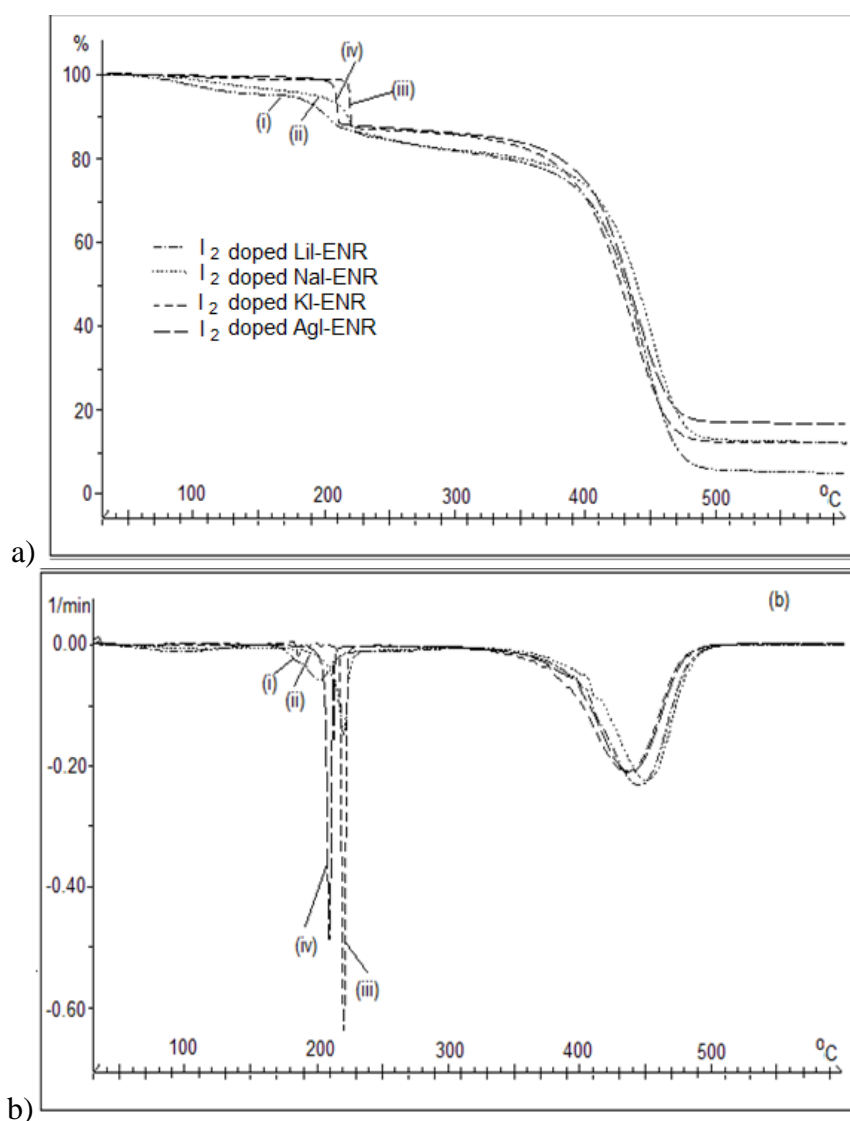


Figure 8. (a) TG and (b) DTG curves for I_2 /MI-ENR PEs where M = (i) Li, (ii) Na, (iii) K and (iv) Ag at a heating rate of $20\text{ }^\circ\text{C min}^{-1}$.

The effect of I_2 loading on the T_{onset} of ENR in doped PEs is illustrated in Figure 9. The T_{onset} increases with the increase in wt% of I_2 in all the doped PEs. For instance, the T_{onset} for AgI-ENR doped with 0, 1, 5 and 10 wt% I_2 was respectively situated at 360, 389, 402 and 408°C. This was attributed to increasing content of the ENR-iodide complex in the PE which causes the PEs to become more stable thermally. As mentioned, the AgI particles catalyze the decomposition of ENR in the undoped systems via effective heat transfer between the particles and polymer. In I_2 /AgI-ENR, an excess amount of I_2 in the system coupled with the formation of ENR-iodide complex may hinder the AgI particles from being in close contact with ENR. This consequently decreases the probability of heat to be effectively transferred to the ENR chains. Thus, the presence of I_2 in the doped AgI-ENR PEs not only depresses the catalytic effect of AgI particles but it also enhances the thermal stability of ENR in the doped PEs.

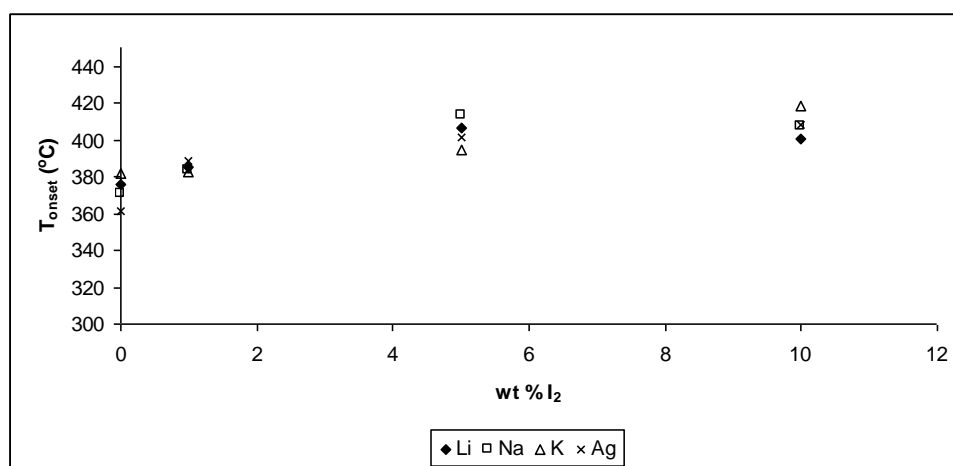


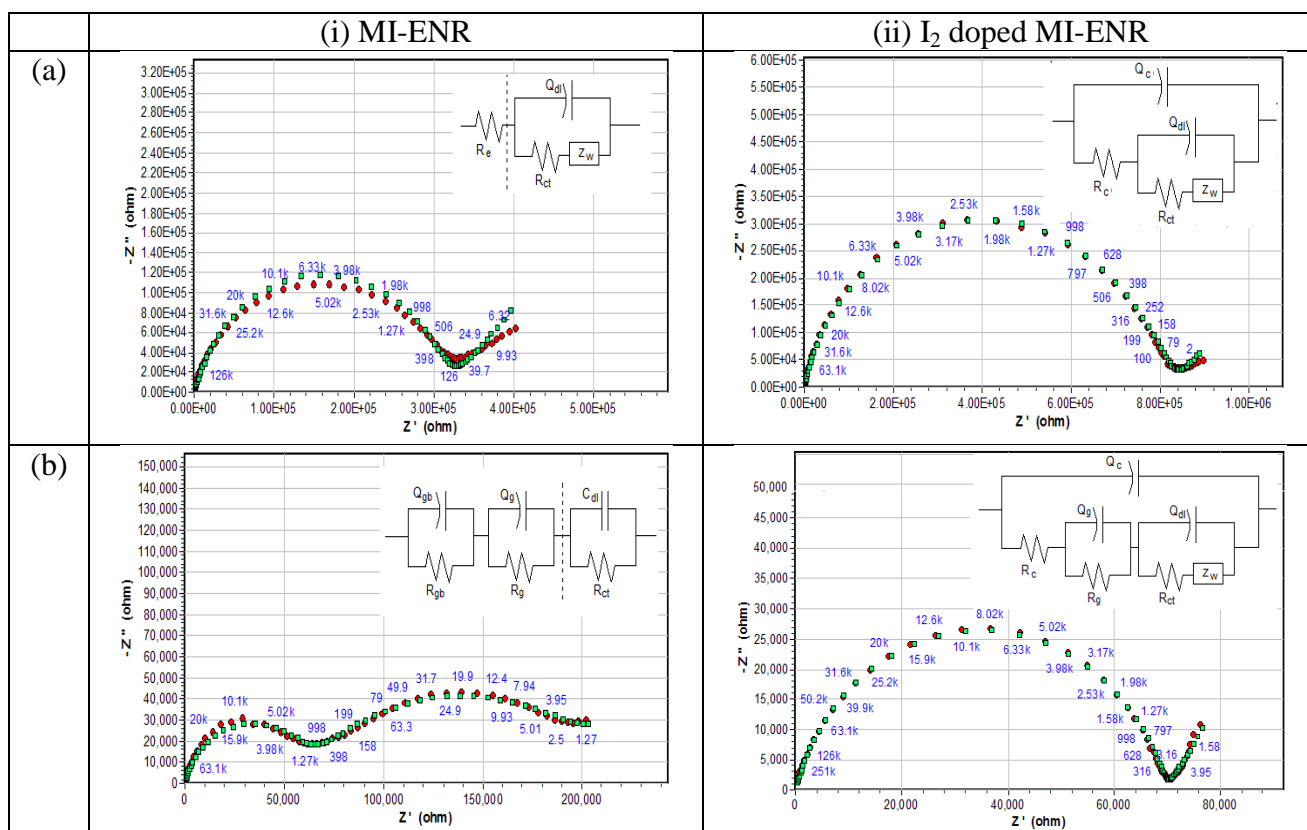
Figure 9. T_{onset} for the various I_2 /MI-ENR PEs as a function of wt% I_2 .

3.4. Impedance Spectroscopy

The Nyquist plot for each PE system and the equivalent circuit is presented in Figure 10. The Nyquist plot for LiI-ENR PE (Figure 10(a)(i)) consists of a skewed semicircle with a spike at low frequency range [26]. The plot best fitted an equivalent circuit that comprises of a resistor denoted by R_e from the contribution of electrolyte resistance and a double layer constant phase element, Q_{dl} parallel to a series connection of charge transfer resistance, R_{ct} and a Warburg element, Z_w . The element of Q_{dl} , R_{ct} and Z_w arises from the double layer at the electrode/electrolyte interface in the system as reported previously [26]. The Nyquist plots for NaI- and KI-ENR PEs are featured in Figure 10(b-c)(i). Typically the plot shows superposition of 3 semicircles. Thus the equivalent circuit is made up from 3 series of resistor and capacitor (RC) components in parallel. The first and second RC components are the contribution from grain boundary (inter-grain) and grain (intra-grain) conduction respectively while the third RC is due to the formation of double layer at the electrode/electrolyte interface. It is worth to note here that the data is better fitted by replacing the ideal capacitor (C) to a non-ideal capacitive component that is the constant phase element (CPE), Q for grain boundary and

grain conduction. This is due to factors like size and inter-particle distance which is not identical throughout the system [51]. The SEM and X-mapping images support the afore-mentioned. An incomplete arch is obtained in the Nyquist plot for AgI-ENR PE system (Figure 10(d)). It is best fitted to a parallel RC circuit. Again here the Q component is used instead of C.

The difference in the feature of the plot and the fitted circuits for these PEs is believed to be closely related to the solubility and morphology of MI in the ENR. As discussed in the early section, the solubility of MI in ENR follows the decreasing trend of $Li > Na > K > Ag$. The LiI is solubilized in the ENR and homogeneously distributed throughout the system. The conduction process is thus ascribed to the resistive movement of charge carriers (Li^+ and I^-) in the bulk electrolyte region, building up of double layer at electrode's surface and their diffusion across the double layer. The NaI and KI are however, partially dissolved in the ENR. There are big and small iodide particles dispersed all over the ENR matrix. Thus the ionic conduction involves the transportation of charge carriers through the inter-grain and intra-grain as well as the double layer. As for the AgI, it is hardly dissolved in the ENR. The AgI particles tend to accumulate into an "island" and is isolated from each other. There is lack of interconnection between the "islands" and therefore the overall conduction process can be deemed as bulk conduction through the intra-grain particles.



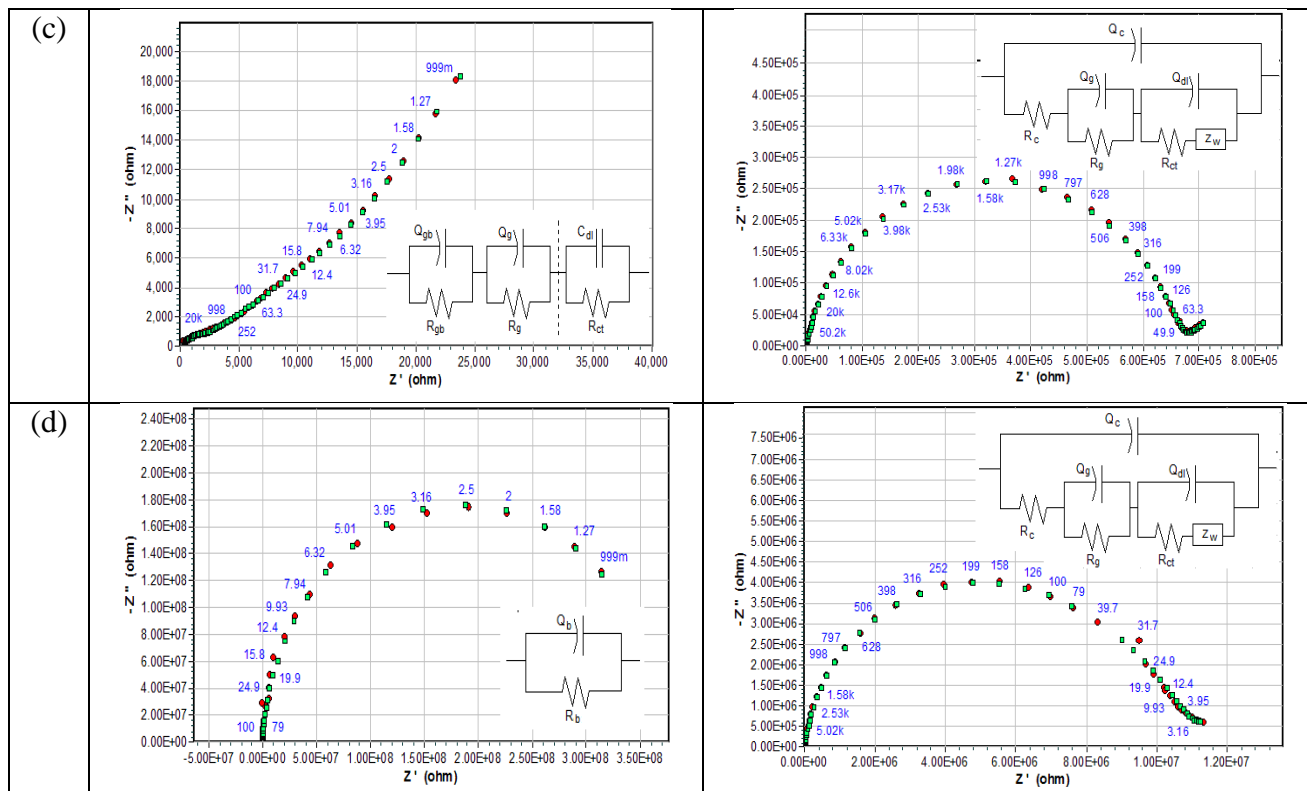


Figure 10. Nyquist plot and the equivalent circuit of 10 wt% MI-ENR PEs and the respective I₂ doped PEs where M = (a) Li, (b) Na, (c) K and (d) Ag [red square = experimental data, green square = fitted data].

The Nyquist plot for all the doped samples are shown in Figure 10(a-d)(i). Typically, they comprise of a skewed semicircle with spur at low frequency range. Even so, the best fitted circuit for I₂ doped LiI-ENR PE is slightly different from the others. The equivalent circuit of doped LiI-ENR shown in Figure 10(a)(ii) consists of a CPE (Q_c) that is parallel to a series of resistor (R_c), CPE (Q_{dl}), resistor (R_{ct}) and Warburg element (Z_w). The nested circuit of Q_{dl} , R_{ct} and Z_w arises from the double layer at the electrode/electrolyte interface as mentioned above, while the Q_c and R_c represent the charge transfer of iodides in the ENR-iodide complexes. On the other hand, another parallel RC components, Q_g and R_g are included into the circuit to better fit the Nyquist plot of doped NaI-, KI- and AgI-ENR systems (Figure 10(b-d)(ii)).

This additional component accounts for the contribution of grain conduction. As shown in SEM and mapping images, the NaI, KI and AgI mostly exist as particles in the PEs due to their poor solubility in ENR.

Therefore, the ionic conduction of doped NaI-, KI- and AgI-ENR PEs also involves the transportation of charge carriers through the MI particles/grains. The Nyquist plots and equivalent circuits for doped PEs are different as compared to the undoped systems. This means that the presence of I₂ in the PEs has changed the conduction mechanism of the PEs.

4. CONCLUSIONS

Except for the LiI, other MI salts showed poor solubility in the ENR. The solubility of MI salts in the ENR followed the decreasing trend of $\text{Li} > \text{Na} > \text{K} > \text{Ag}$. Thus the NaI, KI and AgI were harder to dissociate in the ENR while LiI was mostly existed as ion forms in the PE. An increment of T_g (> 4 °C) was observed upon adding the LiI into the ENR and this was attributed to the pseudo-crosslinking between the Li^+ and ENR. For other iodide salts ($M = \text{Na}, \text{K}$ or Ag), only slight increments of T_g ($\sim 1\text{-}2$ °C) in their respective PEs from pristine ENR was seen, inferring weak or no interaction occurred between the salt and ENR. FTIR spectra also supported the T_g results. The $\overset{\circ}{\underset{\circ}{\text{C}}}\text{-}\overset{\circ}{\underset{\circ}{\text{C}}}$ peak was shifted to a lower wavenumber ($> 3 \text{ cm}^{-1}$) for LiI-ENR. However the position of this peak was almost unchanged (viz. $876\text{-}877 \text{ cm}^{-1}$) for AgI-, KI- and NaI-ENR PEs. SEM and mapping images revealed that the LiI salts were well solvated and homogeneously distributed in the ENR matrix. The NaI, KI and AgI salts were less solvated in the ENR matrix as compared to LiI where some iodide salt particles/aggregates were visible. The thermal stability of ENR in PEs is dependant on the type of metal in MI salt. The alkali metal iodide like Li, Na or K does not greatly influence the thermal stability of ENR. Nevertheless, the presence of AgI thermally destabilized ENR in PE where the T_{onset} was ~ 15 °C lower than pristine ENR. Dissimilarity of the Nyquist plots and its fitted circuit for doped and undoped PEs is believed to be closely related to the solubility and morphology of MI in the ENR. The UV-vis spectra of I_2 -MI-ENR solution indicate the existence of I^- , I_3^- , I_5^- and ENR- I_3^- , ENR- I_5^- complexes in all the I_2 doped PEs. The formation of these ENR/iodide complexes have caused the increment of T_g , enhanced the thermal stability of the ENR and changed the conduction mechanism in doped PEs.

ACKNOWLEDGEMENTS

The authors would like to thank Ministry of Higher Education for the FRGS grant: 203/PKIMIA/6711420 in support of this work. Many thanks to Dr. N.H.H. Abu Bakar and Dr. N.H. Kaus for their insightful comments to this manuscript.

References

1. F.M. Gray, Solid polymer electrolytes: fundamentals and technological applications, VCH Publishers, Inc., New York, US, 1991
2. S. Ahmad, *Ionics*, 15 (2009) 309
3. E.M. Masoud, A.A. El-Bellihi, W.A. Bayoumy, M.A. Mousa, *J. Alloys Comp* 575 (2013) 223
4. R. Idris, M.D. Glasse, R.J. Latham, R.G. Linford and W.S. Schlindwein, *J. Power Sources*, 94 (2001) 206
5. K.H. Teoh, C-S. Lim, C-W. Liew, S. Ramesh, *Ionics*, 21 (2015) 2061
6. A. Ngamaroonchote, C. Chotsuwan, Performance and reliability of cellulose acetate-based gel electrolyte for electrochromic devices, *J. Appl. Electrochem.* (2016) [in press]
7. J. Li, H. Zhu, X. Wang, D.R. MacFarlane, M. Armand, M. Forsyth, *J. Mater. Chem. A*, 3 (2015) 19989
8. Z. Lan, J. Wu, D. Wang, S. Hao, J. Lin, Y. Huang, *Solar Energy*, 80 (2006) 1483
9. J.P.T. Guisao, A.J.F. Romero, *Electrochim. Acta*, 176 (2015) 1447
10. A. Lewandowski, I. Majchrzak, I. Stepniak, *Solid State Ionics*, 132 (2000) 101

11. T.M. Pappenfus, W.A. Henderson, B.B. Owens, K.R. Mann and W.H. Smyrl, *Solid State Ionics*, 171 (2004) 41
12. R. Nadimicherla, R. Kalla, R. Muchakayala, X. Guo, *Solid State Ionics*, 278 (2015) 260
13. R.K. Gupta and H.W. Rhee, *Advanced Opto Electronics*, 2011 (open access, doi:10.1155/2011/102932)
14. M. Vittadello, D.I. Waxman, P.J. Sideris, Z. Gan, K. Vezzu, E. Negro, A. Safari, S.G. Greenbaum and V.D. Noto, *Electrochim. Acta*, 57 (2011) 112
15. C.S.L. Baker, Modified natural rubber, in: A.K. Bhowmick, H.L. Stephens (Eds), *Handbook of elastomers*, 2nd ed., Marcel Dekker, Inc., New York, US, 2001
16. M.D. Glasse, R. Idris, R.J. Latham, R.G. Linford and W.S. Schlindwein, *Solid State Ionics*, 147 (2002) 289
17. W. Klinklai, S. Kawahara, T. Mizumo, M. Yoshizawa, Y. Isono and H. Ohno, *Solid State Ionics*, 168 (2004) 131
18. W. Klinklai, S. Kawahara, E. Marwanta, T. Mizumo, Y. Isono and H. Ohno, *Solid State Ionics*, 177 (2006) 3251
19. S.N. Mohamed, N.A. Johari, A.M.M. Ali, M.K. Harun and M.Z.A. Yahya, *J. Power Sources*, 183 (2008) 351
20. C.H. Chan, H.W. Kammer, *Ionics*, 21 (2015) 927
21. S.A.M. Noor, A. Ahmad, I.A. Talib, M.Y.A. Rahman, *Ionics*, 17 (2011) 451
22. K. Nazir, S.F. Ayub, A.F. Aziz, A.M.M. Ali, M.Z.A. Yahya, *J. Nano Res.* 28 (2014) 163
23. T.K. Lee, F. Afiqah, A. Ahmad, H.M. Dahlan, M.Y.A. Rahman, *J. Solid State Electrochem.* 16 (2012) 2251
24. M.Y.A. Rahman, A. Ahmad, T.K. Lee, Y. Farina, H.M. Dahlan, *J. Appl. Polym. Sci.*, 124 (2012) 2227
25. Q. Lin, Y. Lu, W. Ren, Y. Zhang, *RSC Adv.*, 5 (2015) 90031
26. W.L. Tan, M. Abu Bakar, N.H.H. Abu Bakar, *Ionics*, 19 (2013) 601
27. W.L. Tan, M. Abu Bakar, N.H.H. Abu Bakar, *J. Therm. Anal. Calorim.* 117 (2014) 1111
28. W.L. Tan, M. Abu Bakar, Preparation, characterization, thermal and electrical properties of lithium salt-magnetite/epoxidized natural rubber composite polymer electrolytes, *Ionics* (2016) [doi:10.1007/s11581-016-1658-5]
29. W.L. Tan, M. Abu Bakar, *Am. Eur. J. Sustain. Agric.*, 8 (2014) 111
30. W. Wang, X. Guo and Y. Yang, *Electrochim. Acta*, 56 (2011) 7347
31. H.K. Lee, J. Ismail, H.W. Kammer, M. Abu Bakar, *J. Appl. Polym. Sci.*, 95 (2005) 113
32. Y. Yang, C. Zhou, S. Xu, H. Hu, B. Chen, J. Zhang, S. Wu, W. Liu and X. Zhao, *J. Power Sources*, 185 (2008) 1492
33. E.J. Shin, W.S. Lyoo and Y.H. Lee, *J. Appl. Polym. Sci.*, 123 (2012) 672
34. E.J. Shin, W.S. Lyoo and Y.H. Lee, *J. Appl. Polym. Sci.*, 120 (2011) 1950
35. A.E. Bragg, B.J. Schwartz, *J. Phys. Chem. A*, 112 (2008) 3530
36. N.H. Mohd Hirmizi, M. Abu Bakar, W.L. Tan, N.H.H. Abu Bakar, J. Ismail, C.H. See, Electrical and thermal behavior of copper-epoxy nanocomposites prepared via aqueous to organic phase transfer technique, *J. Nanomaterials*, 2012 (open access, doi: 10.1155/2012/219073)
37. I.L. Validzic, I.A. Jankovic, M. Mitric, N. Bibic, J.M. Nedeljkovic, *Mater. Lett.*, 61 (2007) 3522
38. D.L. Pavia, G.M. Lampman, G.S. Kriz, *Introduction to spectroscopy*, 2nd Ed., Saunders College Publishers, Florida, US, 1996
39. F. Shahidi, Y. Zhong, Chapter 8: Lipid oxidation measurement methods, in F. Shahidi, *Bailey's Industrial Oil and Fat Products*, Vol. 1, *Edible Oil and Fat Products: Chemistry, Properties and Health Effect*, 6th Ed., Wiley Interscience, New Jersey, US, 2005
40. E.M. El-Nemma, *Spectrochim. Acta A*, 60 (2004) 3181
41. K.S. Shin, M. Brezgunova, O. Jeannin, T. Roisnel, F. Camerel, P.A. Senzier, M. Fourmigue, *Cryst. Growth Des.*, 11 (2011) 5337

42. H. Ishida, H. Takahashi, H. Sato, H. Tsubomura, *J. Am. Chem. Soc.*, 92 (1970) 275
43. E.T. Kang, K.L. Tan, K.G. Neoh, H.S.O. Chan, B.T.G. Tan, *Polym. Bull.*, 21 (1989) 53
44. H.G. Cassidy, M. Ezrin, I.H. Updegraff, *J. Am. Chem. Soc.*, 75 (1953) 1615
45. M.H. Khanmirzaei, S. Ramesh, *Ionics* 20 (2014) 691
46. W. Wang, X. Guo, Y. Yang, *Electrochim. Acta* 56 (2011) 7347
47. N.S. Rani, J. Sannappa, T. Demappa, Mahadevaiah, *Ionics* 20 (2014) 201
48. I. Mudrak, *Ionics*, 20 (2014) 83
49. S.Y. Yeo, W.L. Tan, M. Abu Bakar, J. Ismail, *Polym. Degrad. Stab.*, 95 (2010) 1299
50. N. Miyajima, T. Akatsu, O. Ito, R. Sakurovs, S. Shimizu, M. Sakai, Y. Tanabe, E. Yasuda, *Carbon*, 39 (2001) 647
51. M. Quintin, O. Devos, M.H. Delville, G. Campet, *Electrochim. Acta*, 51 (2006) 6426

© 2016 The Authors. Published by ESG (www.electrochemsci.org). This article is an open access article distributed under the terms and conditions of the Creative Commons Attribution license (<http://creativecommons.org/licenses/by/4.0/>).